International Journal of Advances in Applied Sciences (IJAAS)
Vol. 11, No. 2, June 2022, pp. 113~125
ISSN: 2252-8814, DOI: 10.11591/ijaas.v11.i2.pp113-125

Single phase grid interconnected high gain boost converter with soft switching capability

Bogimi Sirisha, Akhilesh Saieni
Department of Electrical, University College of Engineering, Osmania University, Hyderabad (T.S.), India

Article Info

Article history:

Received Oct 26, 2021
Revised Mar 24, 2022
Accepted Apr 20, 2022

Keywords:

Buffer capacitor
Coupled inductor
Grid synchronization
High voltage gain
Passive clamp

ABSTRACT

The grid interconnected application systems require high voltage levels which leads to an efficiency reduction. To overcome this, a new high gain boost converter in association with buffer capacitor, passive clamp recovery circuit to restore leakage energy in coupled inductor is presented. The magnetic field of the linked inductor stores the energy obtained from the supply. The energy is transmitted to the connected load for consumption in further operating modes. A passive clamp network recovers the energy that is stored in the leakage inductance, enhances the gain of voltage, and improves overall system efficiency. The essential feature of this converter is that, high duty ratios are not required to achieve higher voltage gain, hence the reverse recovery problem of the diode is prevented. Moreover, a passive clamp network decreases the voltage stress of the switch, thus a minimum rating switch is used, as a result, the system's total efficiency improves. This converter output is fed as input to a single-phase full-bridge inverter and also synchronized to a single-phase grid. The performance and powers injected are analyzed by connecting a resistive load.

This is an open access article under the CC BY-SA license.

Corresponding Author:

Bogimi Sirisha
Department of Electrical, University College of Engineering, Osmania University
Hyderabad, Telangana 500007, India
Email: sirishab@osmania.ac.in

1. INTRODUCTION

Over the previous two decades, electricity demand increased drastically. This eventually led to excess consumption and depletion of non-renewable fuels. These served as a strong reason for the researchers to shift to solar photovoltaic (PV) panels, wind energy, and other renewable energy sources. But they suffer from major challenges such as, Because of the nonlinear features, efficient use of the source is critical. There is a need to use a maximum power point tracker (MPPT) in order to observe the peak power of a PV module [1]. They are generally operated at low output voltages (typically 30-50 V). As a result, using them for a variety of applications such as grid-connected systems and stand-alone applications becomes challenging due to the high voltage boosting requirement [2].

To increase the voltage level to the required level, a boost converter is required. However, there are certain drawbacks in using traditional DC-DC converters, like, on the supply side, large peak current flows, deteriorating magnetic components such as inductors, and eventually leading to substantial losses. Across the switch, a high voltage appears. The switch on-state resistance is proportional to the square of the voltage rating.

So due to high voltage, the on-state resistance of the switch also increases which increases the conduction losses. Moreover, the operation of the converter at large duty cycles increases the losses in parasitic resistances of components. To increase the voltage level, it is essential to design and study new high gain, efficient boost converters. Some of the following methodologies are implemented to obtain high voltage at converter output and are shown in Figures 1(a)-1(f).

Isolated converters (DC-DC) use high-frequency transformer which causes a large ripple in the current due to leakage inductance and also spikes in voltage across the switch during turn on and are comparatively bulky and costly [1]–[3]. Use of coupled inductors, they utilize the high reluctance core due to air gap and store the energy in magnetizing inductance of the core and uses turns ratio. But they have high leakage inductance increasing losses [4], [5]. Use of interleaved coupled inductor: They use comparatively smaller values of inductances, reducing useful for applications requiring high power [6]. To restore the leakage energy, the active clamp is used. But due to conduction losses in the power switch, generally passive clamp network is preferred [7], [8]. Intermediate storage capacitors can be employed to store energy and transfer it to load and resulting in boosting of voltage at moderate duty ratio values [9]–[11].

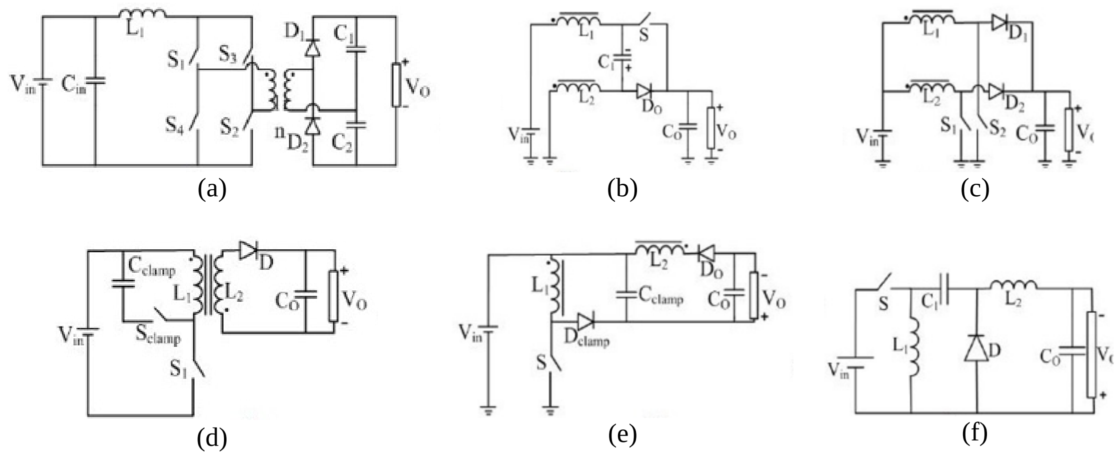

Figure 1. Topology converter output for (a) isolated DC-DC converter, (b) coupled inductor-based, (c) coupled inductor in interleaved arrangement, (d) active clamp-based, (e) passive clamp-based, and (f) energy storage buffer capacitor

2. METHODOLOGY OF NOVEL CONVERTER

Solar PV systems have a modest efficiency (about 14–28%). As a result, in order to maximize the utilization of PV-generated power, an efficient power conversion system is required. The novel converter (boost) topology with maximum gain comprising a coupled inductor (L_1, L_2), one passive clamp recovery network (C_{cl} and DC_l), and a buffer capacitor (C_{int}) shown in Figure 2, is presented.

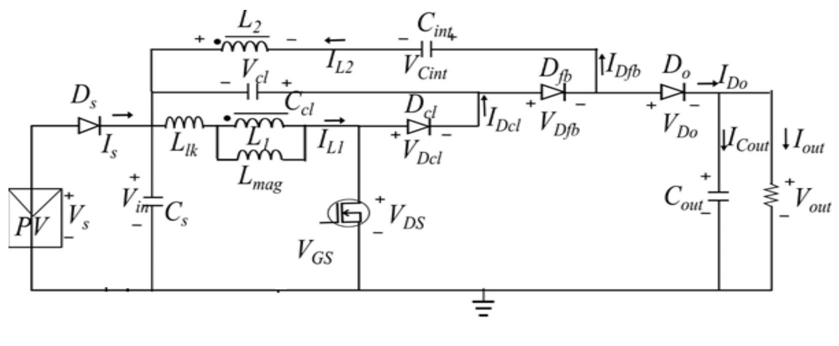

Figure 2. Novel converter (boost DC-DC)

Where L_1 and L_2 are inductances (primary and secondary) of a connected inductor. Passive clamp recovery of L_1 is denoted by C_{cl} and DC_l. The output capacitor is C_{out}, and the output diode is D_o. V_{out} is the voltage across the load. On the secondary side, the buffer capacitor C_{int} and diode D_{fb} are connected.

$$\text{Gain ratio (n) is given by } n = VL2/VL1 \quad (1)$$

2.1. Various operating modes in continuous conduction mode (CCM)

In mode-I, as in Figure 3, the metal oxide semiconductor field-effect transistor (MOSFET) switch is kept on, and current passes by means of a switch and coupled inductor primary winding (L_1), energizing coupled inductor's magnetizing inductance (L_{mag}). DC_l and D_o are reverse biased in this mode, while D_{fb} is forward biased. L_2 and C_{cl} charge the intermediate capacitor C_{int} through D_{fb}. D_{fb} switches off when the voltage across C_{int} equals the sum of the voltages across L_2 and C_{cl}.

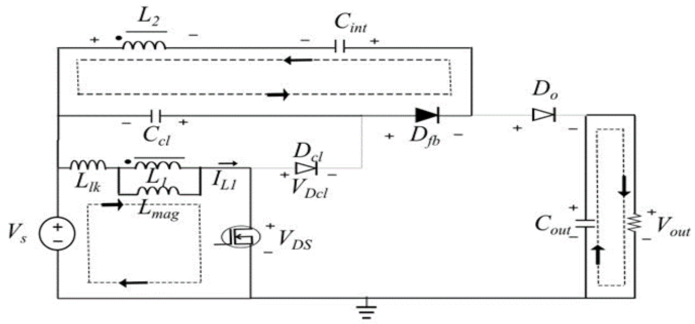

Figure 3. Mode I operation of the novel converter (boost DC-DC)

In mode-II, as shown in Figure 4, the magnetizing current flowing through the primary inductor L_1 charges the switch parasitic capacitance. The feedback diode D_{fb} remains in forwarding bias, current flows through supply, inductance (magnetizing), and parasitic capacitance of MOSFET switch.

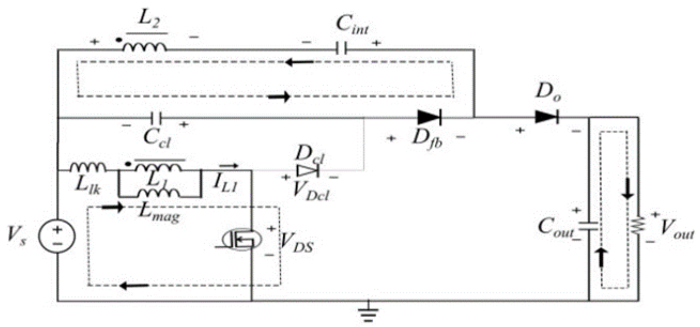

Figure 4. Mode II operation of the novel converter (boost DC-DC)

Diodes DC_l and Do become forward biased in mode-III. D_{fb} is reverse biased. The primary side coupled inductor (L1) leakage energy is collected through DC_l. and stored in the C_{cl}. Furthermore, as illustrated in Figure 5.

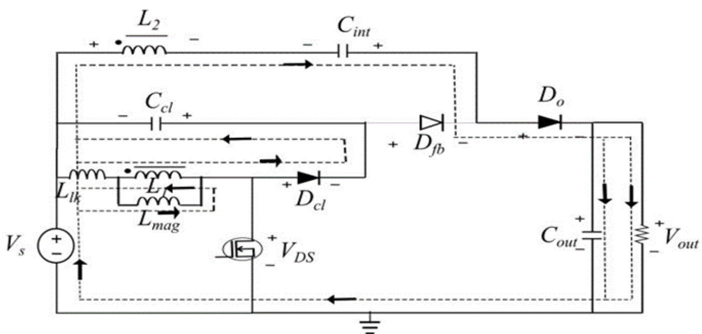

Figure 5. Mode III operation of the novel converter (boost DC-DC)

In Figure 6, Mode-IV begins after the leakage energy from coupled inductor L_1 has been fully recovered. While diode DC_l gets reverse biased, diode D_o remains forward biased. Current flows from input to the load side through inductor L_2, intermediate capacitor C_{int}, and then to the load.

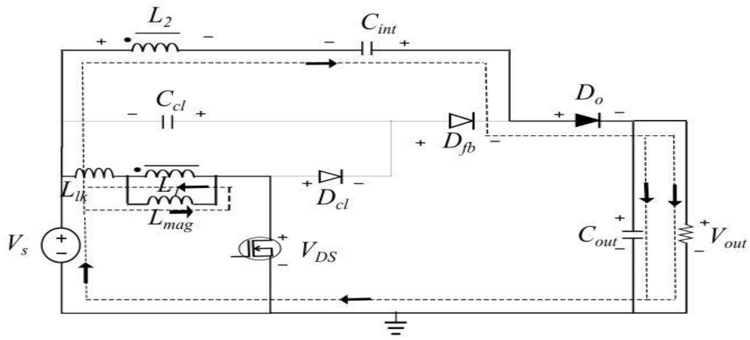

Figure 6. Mode IV operation of the novel converter (boost DC-DC)

Mode-V as seen in Figure 7, the magnetizing current energizes the leakage inductor, while the switch parasitic capacitance discharges. Diodes, DC_l, and D_{fb}, both are reverse biased. When the output diode D_o gets reverse biased and the current direction through inductor L_2 reverses, this mode ceases shown in Figure 7.

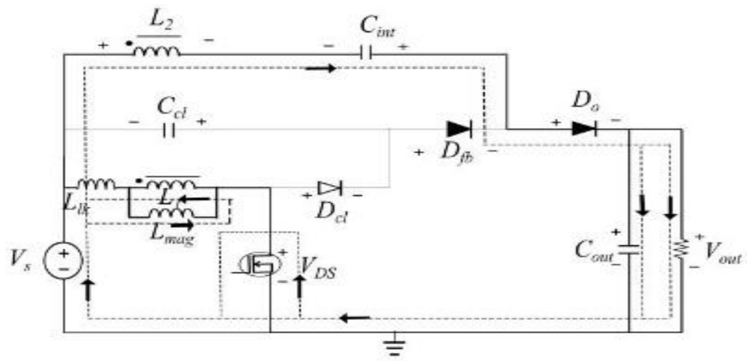

Figure 7. Mode V operation of the novel converter (boost DC-DC)

2.2. Mathematical analysis

The converter's mathematical analysis is required in order to design the components that would be employed in its construction. All of the converter's components are considered to be ideal. During the switch-on state.

$$V_{L1} = V_S \tag{2}$$

$$V_{L2} = V_{Cint} - V_{Ccl} \tag{3}$$

As per gain ratio, $V_{L2} = nV_S$.

During switch off state.

$$V_{L1(off)} = -V_{Ccl} \tag{4}$$

Applying KVL in mode 3 gives $V_{L2} = V_S + V_{Cint} - V_{out}$ (5)

By substituting V_{Cint} from (3), (4),

$$V_{L2} = V_S + nV_S + V_{Ccl} - V_{out}$$
$$V_{L2} = V_S + nV_S - V_{L1(off)} - V_{out} \tag{6}$$

From gain ratio, $V_{L1} = \frac{V_{L2}}{n}$ (7)

By substituting (6) into (7),

$$V_{L1(off)} = \frac{(V_s - V_{L1(off)} + nV_s - V_{out})}{n}$$

$$= \frac{(V_S + nV_S - V_{out})}{(n+1)} \tag{8}$$

Voltage gain, a cross primary inductor L1, on applying voltage-second balance, we get: $V_{L1(on)}.d + V_{L1(off)}.(1-d) = 0$. Substituting (2) and (8), we get: $V_s.d + \frac{(V_S+nV_S-V_{out})}{(n+1)}(1-d) = 0$

$$\frac{V_{out}}{V_S} = \frac{n+1}{1-d} \tag{9}$$

Where d = duty ratio and n= gain ratio.

2.3. Design procedure

A turns ratio is chosen for an input and output voltage requirement, and the duty ratio be computed using (9),

The magnetizing inductance value $L_{mag} = \frac{1}{2} * \frac{V_S*d}{\Delta I_{mag}*f_S}$ (10)

The minimum value of the clamp capacitor $C_{cl} = \frac{I_{mag}*d_{lk}}{\Delta V_{ccl}*f_S}$ (11)

The minimum value of the energy storage capacitor,

$$C_{int} = \frac{I_{mag}*d}{n*\Delta V_{cint}*f_S} \tag{12}$$

The minimum value of the output capacitor,

$$C_{out} = \frac{I_{out}*d}{\Delta V_o*f_S} \tag{13}$$

The minimum required value of output capacitance,

$$C_{out(min)} = \frac{\Delta I_O*xT_S}{0.01V_O} \tag{14}$$

where T_s hold-up time corresponding to load transient of ΔI_o.

For V_s = 35 V, Vout = 350 V, n=4. From (9), $\frac{V_{out}}{V_S} = \frac{(n+1)}{(1-d)}$,We get d = 0.5. From (10), $L_{mag} > \frac{1}{2} * \frac{V_S*d}{\Delta I_{mag}*f_S}$, We get, $L_{mag} > 48\mu H$. From (11), $C_{cl} = \frac{I_{mag}*d_{lk}}{\Delta V_{ccl}*f_S}$ we get C_{cl} = 1μF. From (12), $C_{int} = \frac{I_{mag}*d}{n*\Delta V_{cint}*f_S}$ we get C_{int} = 47μF. From (13), $C_{out} = \frac{I_{out}*d}{\Delta V_{out}*f_S}$ we get C_{out} = 180μF.

With converter parameters as per Table 1, voltages across and current through capacitors, diodes and inductance are obtained as reverse voltage across switch S is $V_{DS} = \frac{V_S}{(1-d)}$ = 70 V, reverse voltage across DC_l is $V_{dcl} = \frac{V_S}{(1-d)}$ = 70 V, peak current through DC_l is $I_{dcl} = \frac{V_{ccl}*d_{lk}}{L_1*f_S}$ = 5.6 A, peak current through L_{mag} is $I_{Lmag} = \frac{V_S}{L_{mag}} * dT_S$ = 7 A, peak current through L_1 is $I_{L1} = \frac{n}{2} * I_{Lmag}$ = 14 A, reverse voltage across D_{fb} is

$V_{dfb} = 2nV_s$ = 280 V, peak current through D_{fb} is $I_{dfb} = \frac{(V_{cint}-V_{ccl})*d}{n*L_2*f_s}$ = 2.25 A, reverse voltage across D_o is $V_{do} = \frac{n}{(1-d)}V_s$ = 280 V, peak current through D_o is $I_{do} = \frac{(V_{out}-V_{ccl}-V_s)*(1-d-d_lk)}{n*L_2*f_s}$ = 1.5 A, voltage across C_{cl} is $V_{ccl} = \frac{d}{1-d}V_s$ = 35 V, and voltage across C_{int} is $V_{cint} = \frac{d(1-n)+n}{(1-d)}V_s$ =175 V.

Table 1. Converter specifications

Source DC voltage	35 V
Output voltage	350 V
Coupled inductor turns ratio	4
Switching frequency	50 kHz
Coupled inductor	Magnetizing inductance L_{mag} = 50 μH
Clamp capacitor	1 µF
Intermediate capacitor	47 µF
Output capacitor	180 µF

The operation of the novel converter is compared with the boost converter in terms of parameters given in Table 2. But in practical application circuits, the inductor in a conventional boost converter will not be perfectly inductive with zero internal resistance due to which the maximum operating duty ratio of the traditional boost converter will be restricted to (0.4-0.6). As a result, we can't operate at 0.9 duty cycle practically, and thus can't obtain a large voltage gain using the traditional converter. The switch drops and switching losses obtained are high. So, it causes high loss switching. Hence it is clear that the novel topology is superior in performance.

Table 2. Comparsion with boost converter (V_s = 35 V, F_{sw} = 50 kHz, L=50 µH, C = 4.7 µF)

	Boost converter (d = 0.9, Ron = 0.068 ohms)	Proposed converter (d = 0.5, Ron = 0.0035 ohms)
Voltage gain	$\frac{Vo}{Vs} = \frac{1}{(1-d)}$ =350 v	$\frac{Vo}{Vs} = \frac{n+1}{1-d}$ = 350 v
Switch loss	$R_{on} * d * \left(\frac{I_{out}}{1-d}\right)^2$ = 6.12 w	$R_{on} * d * \left(\frac{(n+1)I_{out}}{1-d}\right)^2$ =0.18 w
Current through inductor	$\frac{V_s}{L}dT_s$ = 12.6 A	$\frac{V_s}{L}dT_s$ = 7 A
Switch voltage drop	$\frac{V_s}{1-d}$ = 35/1-0.9 = 350 v	$\frac{V_s}{1-d}$ = 35/1-0.5 = 70 v
Leakage energy	$\frac{1}{2}C\left(\frac{V_s}{1-d}d\right)^2$ =0.23 w	$\frac{1}{2}C\left(\frac{V_s}{1-d}d\right)^2$ = 0.004 w

3. GRID SYNCHRONIZATION

The following Figures 8 and 9 depict the complete block diagram of the system with synchronization and resistive load. The grid current is sensed and converted into two orthogonal signals I_α, I_β by introducing a transport delay of 90°.

$$I_\alpha = A\ \sin(\omega t + \phi) \tag{15}$$

$$I_\beta = A\ \sin\left(\omega t + \phi - \frac{\pi}{2}\right) = \ -A\ \cos(\omega t + \phi) \tag{16}$$

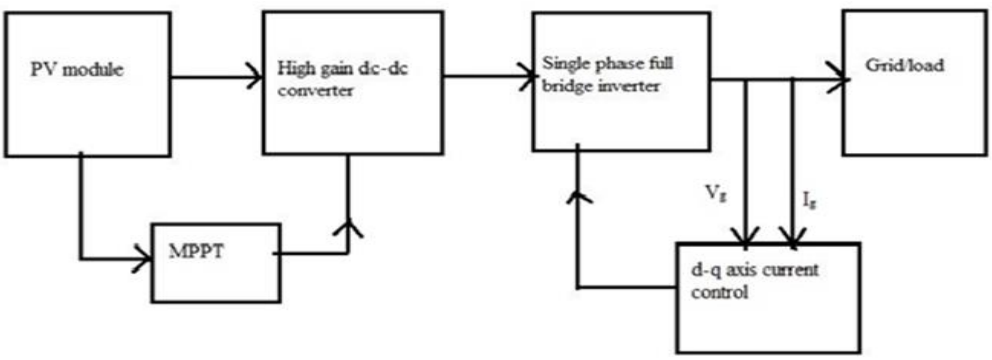

Figure 8. Block diagram of entire grid-connected system

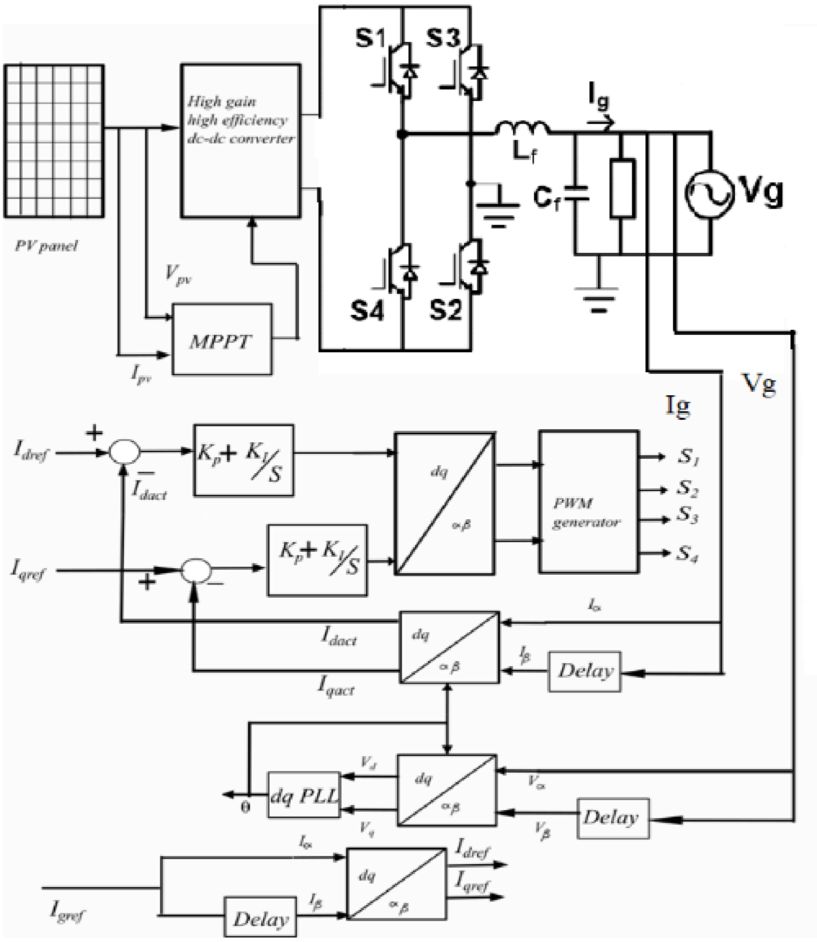

Figure 9. Proposed control scheme for management of power flow of a grid connected PV system

The signals are transformed to dq reference frame to get corresponding current signals by using parks transformation.

$$I_{dq} = \begin{bmatrix} I_d \\ I_q \end{bmatrix} = T\, I_{\alpha\beta} = \begin{bmatrix} \sin\omega t & -\cos\omega t \\ \cos\omega t & \sin\omega t \end{bmatrix} \begin{bmatrix} I_\alpha \\ I_\beta \end{bmatrix} \quad (17)$$

$$i_\alpha = A\, \sin(\omega t + \phi) \sin\omega t + A\, \sin\left(\omega t + \phi - \frac{\pi}{2}\right) (-\cos\omega t) = A\cos\phi \quad (18)$$

$$i_\beta = A \sin(\omega t + \phi)\, \cos\omega t + A\, \sin\left(\omega t + \phi - \frac{\pi}{2}\right) (\sin\omega t) = A\sin\phi \quad (19)$$

The grid voltage V_g is given as input to the phase-locked loop to get the corresponding phase angle. The actual current signals are compared with current signals obtained from the grid reference current [12]–[25]. The obtained errors are minimized using proportional-integral controllers. The output signals are transformed into a stationary frame using the inverse parks transform shown.

$$I_{\alpha\beta} = \begin{bmatrix} I_\alpha \\ I_\beta \end{bmatrix} = T^{-1} I_{dq} = \begin{bmatrix} \sin\omega t & \cos\omega t \\ \cos\omega t & -\sin\omega t \end{bmatrix} \begin{bmatrix} I_d \\ I_q \end{bmatrix} \quad (20)$$

The output generates the required reference wave to the pulse width modulation (PWM) generator and compared with the carrier wave and generates the switching pulses and thus controlling the output voltage of the full-bridge inverter. Figure 10 shows the complete simulation model of the system with detailed description parameters in Table 3.

4. RESULTS AND DISCUSSION

The converter is analyzed in simulation with a matrix laboratory (MATLAB/Simulink) environment. The waveforms of current and voltage supplied by the PV array are shown in Figure 11. Outputs of switch voltage, Magnetizing current, voltage through diode, and voltages of clamped capacitors during various operational modes are shown in Figure 12 and Figure 13. Efficiency at full load is obtained as 94% shown in Figure 14.

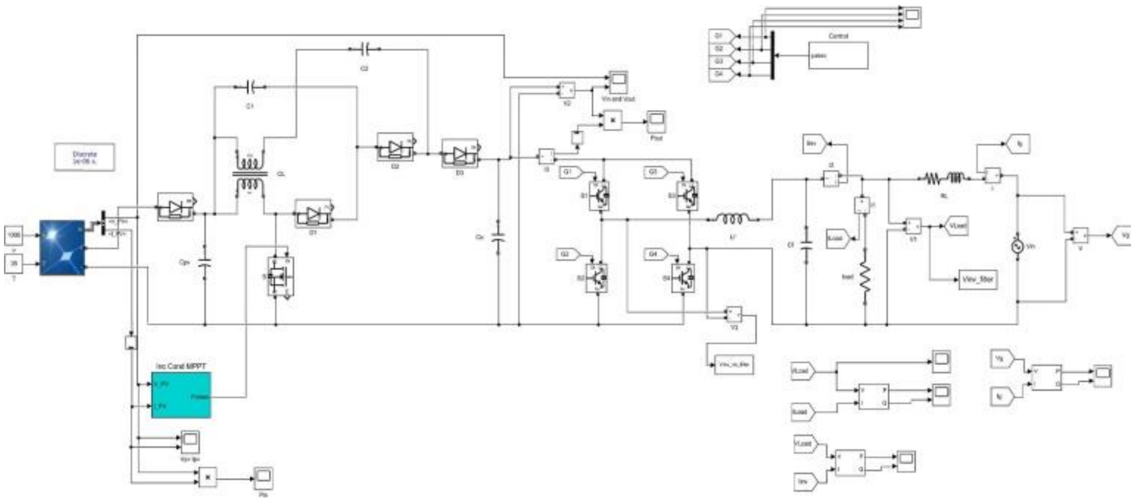

Figure 10. Simulation model of the overall system

Table 3. Values of simulation

Parameters	Their Values
Switching frequency	5 kHz
Couple inductor turns ratio	4
Filter inductance	1 mH
Filter capacitor	5 µF
AC peak voltage	324 V
Resistive load active power	500 W
Resistive load reactive power	0 VAR
Module peak power	240 W
Open circuit module voltage(V_{oc})	51 V
Short circuit module current(I_{sc})	6.3 A
MPP voltage of module(V_{mp})	42.8 V
MPP current of module(i_{mp})	5.6 A
Peak power of array (P_{mp})	1200 W
Open circuit array voltage(V_{oc})	51 V
Short-circuit array current(I_{sc})	31.5 A
MPP voltage of array(V_{mp})	42.8 V
MPP current of array(I_{mp})	28.03 A

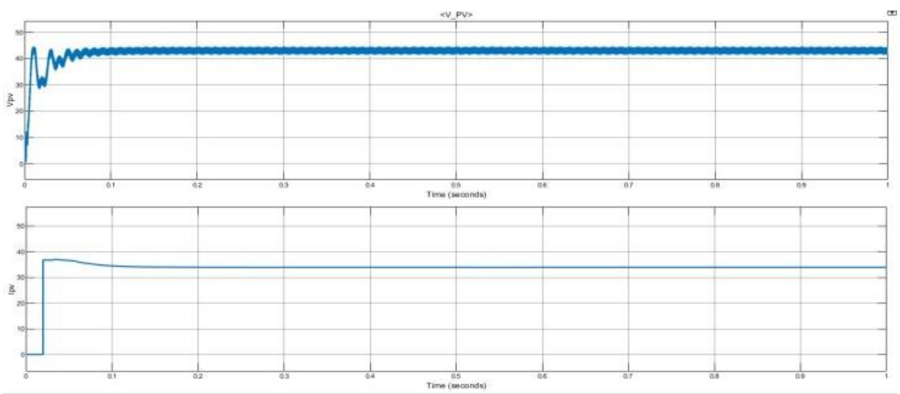

Figure 11. PV voltage-current waveforms

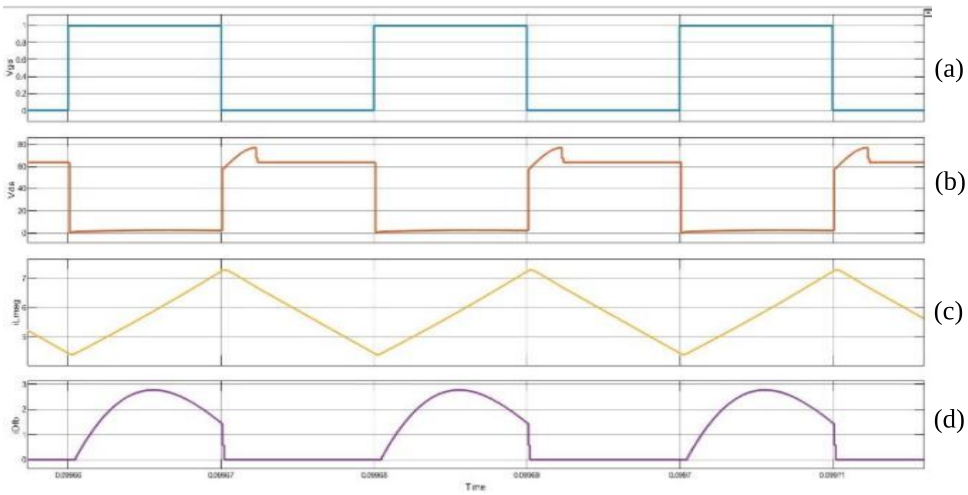

Figure 12. Waveforms of (a) gate to switch voltage, (b) switch voltage, (c) magnetizing current, and (d) current through feedback diode

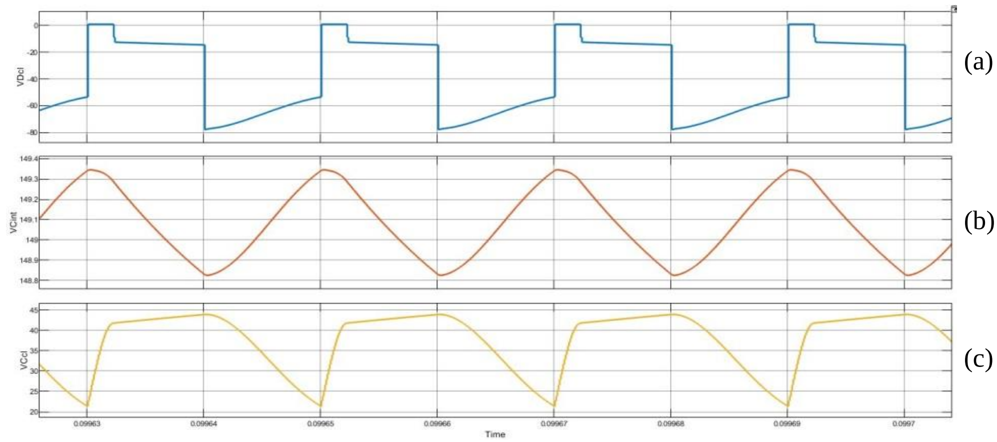

Figure 13. Waveforms of (a) voltage of clamp diode, (b) voltage of intermediate capacitor, (c) voltage of clamp capacitor

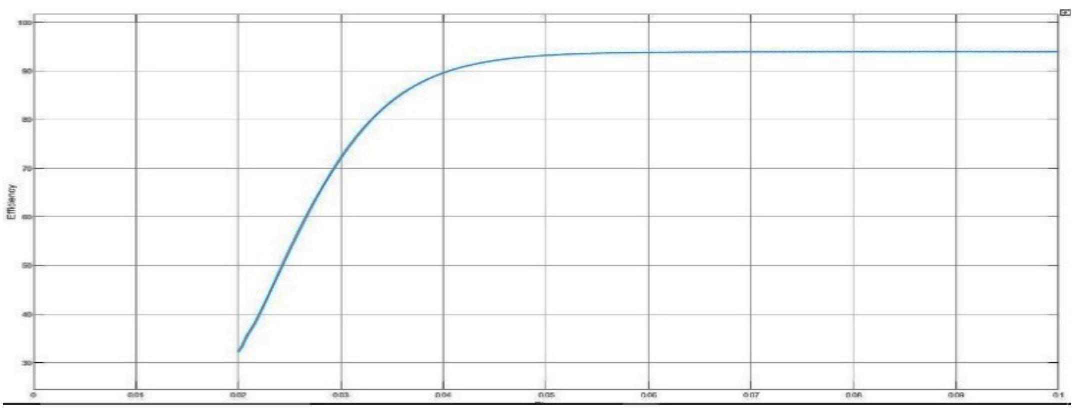

Figure 14. The efficiency of the proposed converter

Filter inductance is designed based on limiting ripple in load current to 20 % of the rated current.

$$L = \frac{V_{dc}}{4 f_{sw} \Delta I_{ppmax}} = 1 \text{ mH} \tag{21}$$

Underrated conditions, the reactive power that can be absorbed must be restricted to 5% of rated power, therefore filter capacitance is calculated accordingly.

$$Q = \frac{V^2}{X_c} = V^2.2\pi f C \tag{22}$$

$$C = 5\ \mu\text{F} \tag{23}$$

Table 4 shows total harmonic distortion (THD) before and after the inductor and capacitor (LC) filter. By employing the filter, the square wave output wave of the inverter is converted to a nearly sinusoidal signal and higher-order harmonics are eliminated. THD obtained is 4.62%, and fast Fourier transform (FFT) analysis is presented in Figure 15 and Figure 16.

Table 4. Total harmonic distortion (THD) before and after inductor and capacitor (LC) filter

Parameters	THD
Before filter	52.08%
After filter	4.62%

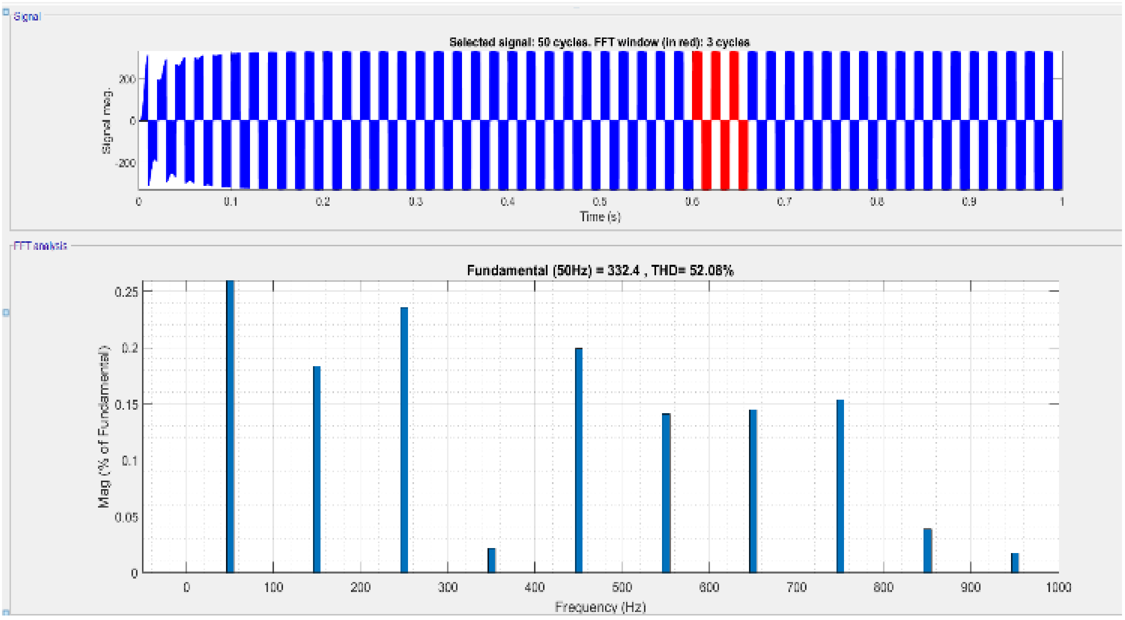

Figure 15. THD of voltage waveform without LC filter

The system is tested during both light load and overload conditions. During light load conditions, the excess power output from the inverter is fed to the grid and hence the grid power appears as negative in the waveform. During overload conditions, the inverter supplies a portion of the load's required power, while the grid supplies the remaining active power, as indicated in Figure 17, Figure 18, and Figure 19. Table 5 shows the power balance between load and grid.

Table 5. The power balance between load and grid

Total inverter power(1100W)	Power supplied by inverter	Grid power
a) Light load (500 W)	500 W	-600 W (injected to grid)
b) Overload (1800 W)	1100 W	700 W (injected by grid)

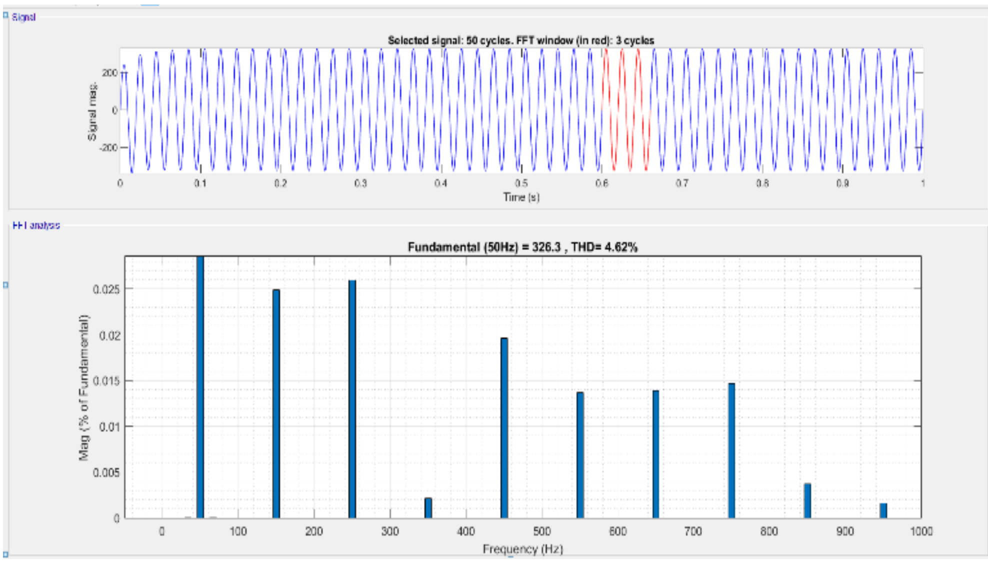

Figure 16. THD of voltage waveform with LC filter

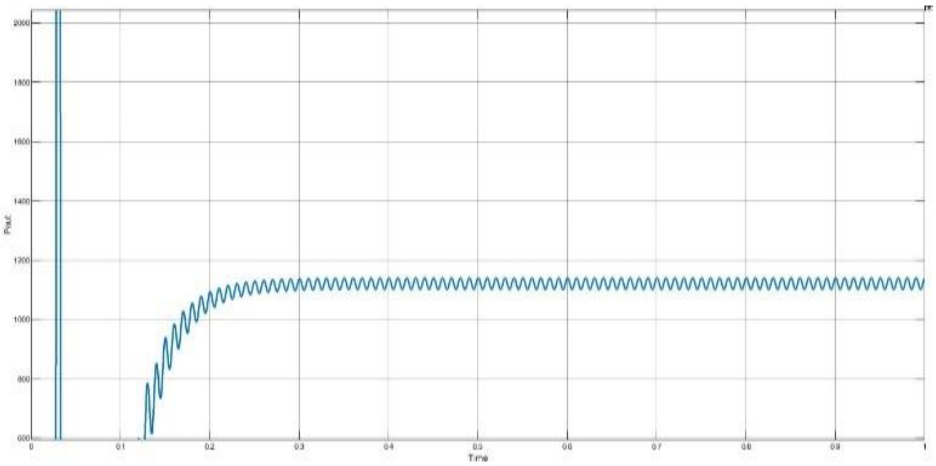

Figure 17. Power output from the inverter

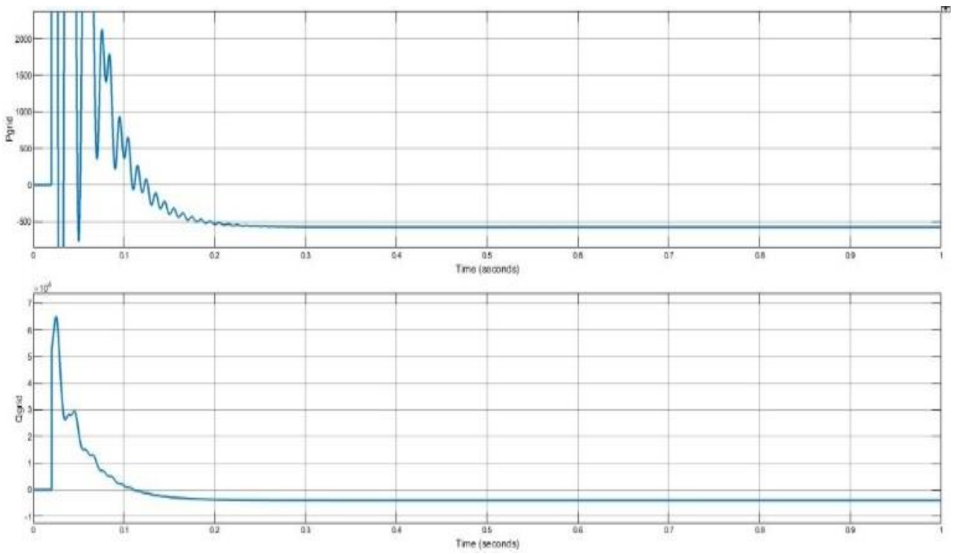

Figure 18. Power injected to the grid (light load conditions)

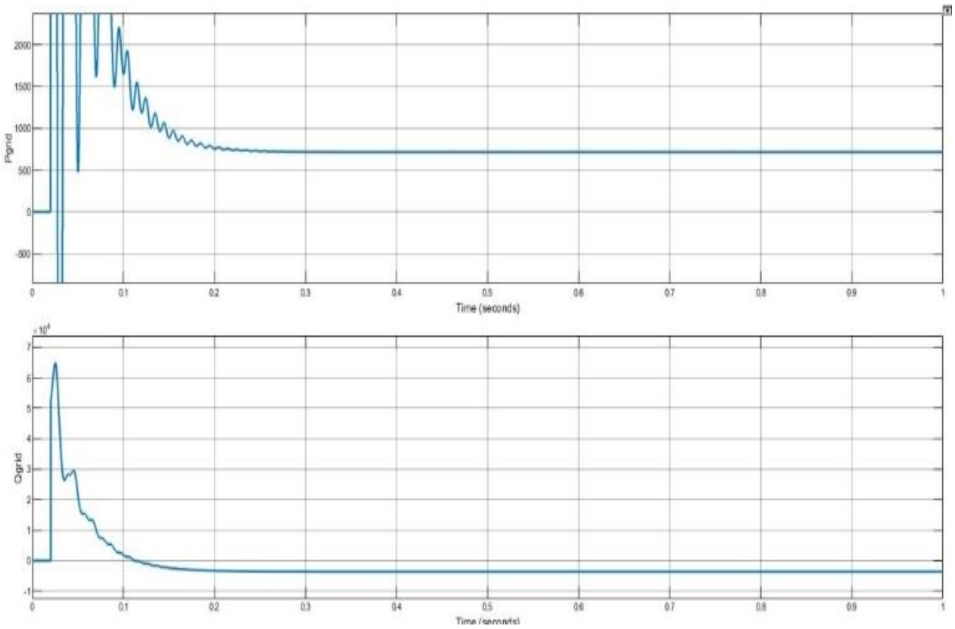

Figure 19. Power injected by the grid to load (overload conditions)

5. CONCLUSION

A boost converter with a large gain was implemented for low and medium-voltage source applications. High voltage gain is obtained at lower duty cycles with minimum switching is obtained. The converter is fed to a single-phase full-bridge inverter, which is then interconnected to the grid. The system is synchronized to the grid by using d-q axis current control. The proposed converter's performance is verified in a simulation environment, and the findings are presented. The switching pulses to the inverter are generated from the pulse generator based on d-q axis control. Output voltages and power with and without LC filter are observed at light load and overload conditions and THD is calculated.

REFERENCES

[1] B. Sirisha and S. Akhilesh, “High efficient and high gain boost converter with soft switching capability connected to grid using dq axis current control,” *Bulletin of Electrical Engineering and Informatics*, vol. 11, no. 2, pp. 624–635, 2022, doi: 10.11591/eei.v11i2.3358.

[2] M. Prudente, L. L. Pfitscher, G. Emmendoerfer, E. F. Romaneli, and R. Gules, “Voltage multiplier cells applied to non-isolated DC-DC converters,” *IEEE Transactions on Power Electronics*, vol. 23, no. 2, pp. 871–887, 2008, doi: 10.1109/TPEL.2007.915762.

[3] B. Sirisha and M. A. Nazeemuddin, “A novel five-level voltage source inverter interconnected to grid with srf controller for voltage synchronization,” *Bulletin of Electrical Engineering and Informatics*, vol. 11, no. 1, pp. 50–58, 2022, doi: 10.11591/eei.v11i1.3274.

[4] P. Xuewei and A. K. Rathore, “Novel bidirectional snubberless naturally commutated soft-switching current-fed full-bridge isolated DC/DC converter for fuel cell vehicles,” *IEEE Transactions on Industrial Electronics*, vol. 61, no. 5, pp. 2307–2315, 2014, doi: 10.1109/TIE.2013.2271599.

[5] A. F. Witulski, “Introduction to Modeling of Transformers and Coupled Inductors,” *IEEE Transactions on Power Electronics*, vol. 10, no. 3, pp. 349–357, 1995, doi: 10.1109/63.388001.

[6] J. Xu, “Modeling and analysis of switching DC-DC converter with coupled-inductor,” *China 1991 International Conference on Circuits and Systems*, pp. 717–720, 1991, doi: 10.1109/ciccas.1991.184459.

[7] F. S. Garcia, J. A. Pomilio, and G. Spiazzi, “Modeling and control design of the interleaved double dual boost converter,” *IEEE Transactions on Industrial Electronics*, vol. 60, no. 8, pp. 3283–3290, 2013, doi: 10.1109/TIE.2012.2203770.

[8] A. D. Dwivedi, G. Srivastava, S. Dhar, and R. Singh, “A decentralized privacy-preserving healthcare blockchain for IoT,” *Sensors (Switzerland)*, vol. 19, no. 2, 2019, doi: 10.3390/s19020326.

[9] K. C. Tseng and C. C. Huang, “High step-up high-efficiency interleaved converter with voltage multiplier module for renewable energy system,” *IEEE Transactions on Industrial Electronics*, vol. 61, no. 3, pp. 1311–1319, 2014, doi: 10.1109/TIE.2013.2261036.

[10] S. Lee, P. Kim, and S. Choi, “High step-up soft-switched converters using voltage multiplier cells,” *IEEE Transactions on Power Electronics*, vol. 28, no. 7, pp. 3379–3387, 2013, doi: 10.1109/TPEL.2012.2227508.

[11] M. El malah, A. Ba-Razzouk, M. Guisser, E. Abdelmounim, and M. Madark, “Backstepping based power control of a three-phase single-stage grid-connected PV system,” *International Journal of Electrical and Computer Engineering*, vol. 9, no. 6, pp. 4738–4748, 2019, doi: 10.11591/ijece.v9i6.pp4738-4748.

[12] A. Rahnamaei and M. Salimi, “A Novel Grid Connected Photovoltaic System,” *Bulletin of Electrical Engineering and Informatics*, vol. 5, no. 2, pp. 133–143, 2016, doi: 10.11591/eei.v5i2.523.

[13] B. Sirisha, N. Susheela, and P. Satishkumar, "Three phase two leg neutral point clamped converter with output DC voltage regulation and input power factor correction," *International Journal of Power Electronics and Drive Systems*, vol. 2, no. 2, pp. 138–150, 2012, doi: 10.11591/ijpeds.v2i2.226.

[14] I. Setiawan, M. Facta, Hermawan, T. Andromeda, M. H. Purnomo, and Taufik, "Sinusoidal Current Control Strategies for Single Phase Grid-Connected Renewable Power Generation Systems," *7th International Conference on Information Technology, Computer, and Electrical Engineering, ICITACEE 2020 - Proceedings*, pp. 241–246, 2020, doi: 10.1109/ICITACEE50144.2020.9239212.

[15] B. Sirisha and P. S. Kumar, "SVPWM Based Generalized Switching Schemes for Seven Level DCMLI Including over Modulation Operation - FPGA Implementation," *IEEE Region 10 Annual International Conference, Proceedings/TENCON*, vol. 2019-Octob, pp. 2135–2142, 2019, doi: 10.1109/TENCON.2019.8929380.

[16] B. Sirisha and P. S. Kumar, "A Simplified Space Vector Pulse Width Modulation Method Including Over Modulation Operation for Five Level Cascaded H-bridge Inverter with FPGA Implementation," *International Journal of Power Electronics and Drive Systems (IJPEDS)*, vol. 8, no. 3, p. 1203, Sep. 2017, doi: 10.11591/ijpeds.v8.i3.pp1203-1211.

[17] J. H. Lee, T. J. Liang, and J. F. Chen, "Isolated coupled-inductor-integrated DC-DC converter with nondissipative snubber for solar energy applications," *IEEE Transactions on Industrial Electronics*, vol. 61, no. 7, pp. 3337–3348, 2014, doi: 10.1109/TIE.2013.2278517.

[18] Y. P. Hsieh, J. F. Chen, T. J. Liang, and L. S. Yang, "Novel high step-Up DC-DC converter for distributed generation system," *IEEE Transactions on Industrial Electronics*, vol. 60, no. 4, pp. 1473–1482, 2013, doi: 10.1109/TIE.2011.2107721.

[19] M. Das and V. Agarwal, "A novel, high efficiency, high gain, front end DC-DC converter for low input voltage solar photovoltaic applications," *IECON Proceedings (Industrial Electronics Conference)*, pp. 5744–5749, 2012, doi: 10.1109/IECON.2012.6389046.

[20] B.Sirisha, "A grid interconnected nested neutral point clamped inverter with voltage synchronization using synchronous reference frame controller," *International Journal of Applied Power Engineering (IJAPE)*, vol. 10, no. 4, pp. 364–372, 2021, doi: 10.11591/ijape.v10.i4.pp364.

[21] M. Das and V. Agarwal, "Design and Analysis of a High-Efficiency DC-DC Converter with Soft Switching Capability for Renewable Energy Applications Requiring High Voltage Gain," *IEEE Transactions on Industrial Electronics*, vol. 63, no. 5, pp. 2936–2944, 2016, doi: 10.1109/TIE.2016.2515565.

[22] B. Crowhurst, E. F. El-Saadany, L. El Chaar, and L. A. Lamont, "Single-phase grid-tie inverter control using DQ transform for active and reactive load power compensation," *PECon2010 - 2010 IEEE International Conference on Power and Energy*, pp. 489–494, 2010, doi: 10.1109/PECON.2010.5697632.

[23] R. Zhang, M. Cardinal, P. Szczesny, and M. Dame, "A Grid Simulator with control of single-phase power converters in D-Q rotating frame," *PESC Record-IEEE Annual Power Electronics Specialists Conference*, vol. 3, pp. 1431–1437, 2002, doi: 10.1109/PSEC.2002.1022377.

[24] A. B. Shitole *et al.*, "Grid Interfaced Distributed Generation System with Modified Current Control Loop Using Adaptive Synchronization Technique," *IEEE Transactions on Industrial Informatics*, vol. 13, no. 5, pp. 2634–2644, 2017, doi: 10.1109/TII.2017.2665477.

[25] A. Hota, S. K. Bhuyan, and P. K. Hota, "Modeling Simulation of Photovoltaic System Connected to Grid using Matlab," *Proceedings of the 2020 International Conference on Renewable Energy Integration into Smart Grids: A Multidisciplinary Approach to Technology Modelling and Simulation, ICREISG 2020*, pp. 16–21, 2020, doi: 10.1109/ICREISG49226.2020.9174192.

BIOGRAPHIES OF AUTHORS

Bogimi Sirisha She holds a B.E. in Electrical Engineering from Osmania University, M. Tech Power Eelectronics from JNTUH in 2003, and a Ph.D. degree from Osmania University 2018. She has over 16 years of experience in research and teaching and is currently employed as an Associate Professor in Electrical Department, Engineering College, Osmania University, Hyderabad, INDIA. She has published various articles in international and national journal publications and conferences. Multilevel Inverters, Power Electronics and Drives, Renewable Energy Applications and Special Electrical Machines are among her research interests. Osmania University awarded her a Ph.D. in the field of multilevel inverters.

Akhilesh Saieni He holds a B.E. in Electrical Engineering, M.E. in Industrial Drives and Control from University College of Engineering (A), Osmania University, Hyderabad, Telangana, India.His field of interests are Renewable energy resources and its applications, Power electronics and drives. He can be contacted at email: saieniakhilesh@gmail.com